ASEAN Engineering Journal

Full Paper

ON A GENERALIZED INPUT SHAPING FOR RESIDUAL VIBRATION SUPPRESSION IN FLEXIBLE SYSTEM WITH NONLINEAR SPRING AND DAMPER

Ittidej Moonmanngmee*, Withit Chatlatanagulchai

Control of Robot and Vibration Laboratory, Department of Mechanical Engineering, Faculty of Engineering, Kasetsart University, Bangkok 10900, Thailand

Article history
Received
28 December 2023
Received in revised form
06 June 2024
Accepted
16 July 2024
Published online
31 May 2025

*Corresponding author
ittidej.m@ku.th

Graphical abstract

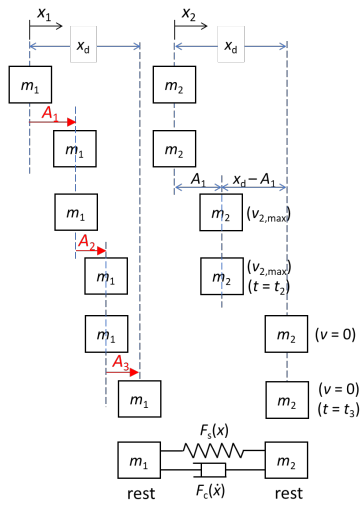

Abstract

Suppression of residual vibrations in position control of flexible systems is a challenging problem, especially in the presence of high nonlinearities or diverse operating points. Input shaping, a technique for designing shaped commands to minimize system residual vibration during point-to-point movements, is crucial. Traditional input shapers like zero-vibration and zero-vibration-and-derivative shapers, designed based on the superposition principle, perform well for linear systems but have limitations in highly nonlinear systems. This paper revisits nonlinear input shapers, including three-impulse and robust shapers, providing a comprehensive energy-based analysis. Additionally, a novel fast three-impulse shaper is proposed to improve the time-delay of traditional input shapers. The amplitudes and time locations of all designed shapers are proven in the same closed-form solution for the undamped case, suitable for analyzing sensitivity to variations in plant parameters. Demonstrations on a two-mass flexible system with nonlinear spring and damper show that the proposed fast-three shaper outperforms the two-impulse shaper in robustness, with similar performance in rise time. However, robust shapers, while slower, exhibit superior robustness as increasing impulse numbers decrease residual total energy. The effect of nonlinear damping force is demonstrated in simulations, providing suggestions for designing robust shapers for damped flexible systems.

Keywords: Residual vibration control, input shaping, flexible systems, Duffing nonlinearity, nonlinear systems

1.0 INTRODUCTION

Control of residual vibration in flexible systems is a crucial problem in many engineering applications, especially in the position control of electro-mechanical systems, such as cranes with swinging payloads [1], industrial robot manipulators [2], X-Y linear motion stage [3], torsional vibrations in aircraft drivetrains [4], eliminating bouncing in electrohydraulic system with elastic manipulator [5], micro-electro-mechanical-system (MEMS) contact switches [6], and piezoelectric/dielectric elastomer actuators [7]. Several reasons that the residual vibration emerged in such systems, such as the inclusion of mechanical flexible parts in the system or the design of lightweight structure design, which severely degrades performance of positioning accuracy. An effective methodology to mitigate residual vibration is utilizing feedforward/feedback control, which is cheaper, more flexible to design, and can reduce the system settling time, than using the external passive devices such as dashpots.

There are numerous techniques in linear/nonlinear control theory that can be applied to control flexible systems. However, an effective method is to design appropriate command input, i.e., by input shaping so as not to excite the vibration mode of the system. The shaped command input under the name input shaping has been proposed for decades [8] and is still widely used to present day. The well-known input shapers, including Zero-Vibration (ZV) shaper, Zero-Vibration-Derivative (ZVD) shaper were later developed based on linear models to handle uncertainties in mode parameters [9]. The input shaping

technique is implemented by convolving a desired system input with a specific sequence of impulses. With an appropriate design of impulse amplitudes and times, an impulse response of the flexible system can be cancelled by another impulse response, resulting in zero residual vibration when the system moves from point-to-point.

Over the last few decades, vibration reduction strategies by input shaping have been classified into four major categories: 1) Improvement or development of novel input shapers to solve specific problems, such as actuator saturation limits [10], non-zero initial state movement [11, 12, 13, 14], configuration-dependent dynamics [2] and [15], time-dependent system frequency [16, 17], and flexible systems with nonlinearity [18, 19]. 2) Integration of existing linear input shaping with optimal control to solve time-optimal or fuel-optimal problems [20, 21, 22, 23]. 3) Inclusion of input shaper into a control system to enhance control and robust performance, such as the improvement of speed performance in backstepping model matching [24], using quantitative feedback controller with model reference to handle a large plant uncertainty [25]. 4) Implementation of designed shaping/control to challenging applications, such as human control of crane [26], structural health monitoring [27]. This work primarily focuses on the analysis and development of nonlinear input shapers in a general closed form without using a feedback controller, known as open-loop input shaping, and thus belongs to the first category. However, this proposed nonlinear shaper can be used in a feedback control system in practice.

Most recent works refer to a linear or linearized plant model, allowing the existing basic linear shapers to be applied. These shapers are designed using the natural frequencies and damping ratios of the linearized model at specific operating points, while nonlinearities are treated as plant uncertainties and handled by controllers. However, this approach may be unacceptable when the plant exhibits strong nonlinearities, leading to significant deviations between the linearized model and the actual nonlinear plant. In such cases, gain scheduling, interpolation, or adaptive techniques may be useful but will simultaneously increase the complexity of the design procedures. Compared to the extensive literature on linear input shaper design, limited attention has been directed towards the direct design of nonlinear input shapers. Some works utilized phase portrait tools from nonlinear systems to design nonlinear shapers [28, 29, 30, 31]. However, the limitation of phase portraits, which can only illustrate a two-dimensional phase plane, restricts their application to single-degree-of-freedom dynamics, rendering them unsuitable for systems with dynamic coupling. Others emphasized the concept of the work-energy principle to design nonlinear shapers. In [32, 33, 34], the conservation of energy principle was applied to design nonlinear input shapers for configuration-dependent dynamics with nonlinearities in spring stiffness and damping. These works considered both displacement and force excitations through a single mass system. Following this approach, [18] and [35] presented nonlinear input shapers using two-step and three-step applied forces for a mass-spring system with Duffing nonlinear spring stiffness. They proved that within the linear limit, these shapers can be reduced to the traditional ZV and ZVD shapers, respectively. However, for force excitation configurations, they cannot be generally applied to flexible systems with two degrees of freedom. A more suitable configuration involves considering systems excited by displacement. In [19], a two-mass rigid-flexible system with nonlinear spring and damper was used to demonstrate designed nonlinear shapers, such as the two-impulse shaper, robust input shaper, and negative input shaper. Despite this work opening up the challenge of designing nonlinear shapers in the general case, several fundamental issues persist. The explicit expressions for determining all parameters of a robust nonlinear shaper should be more concise and clarified. Furthermore, the physical intuitiveness of designing shaper parameters through an energy perspective has not been developed, impacting the potential for analysing the sensitivities against parameter variations.

This paper draws inspiration from previous works [12] and [18, 19], utilizing the same energy analysis approach to design nonlinear input shapers directly from their nonlinear dynamics. A two-degrees-of-freedom (DOF) flexible system with Duffing nonlinearity serves as a benchmark to demonstrate the designed shapers. This system encompasses the majority of actual rigid-flexible systems with two-degrees-of-freedom, such as flexible-joint robots, cart-pendulum systems, gantry cranes, etc. However, these systems are considered as a single mode of vibration in their flexible part, which is uncontrolled directly but is excited by the displacement of the rigid-body part of the flexible system. The shaped reference position from the shaper will be designed solely for the rigid-body part to track using a feedback controller. The first part of this paper is dedicated to presenting related work in [18, 19], involving the design of nonlinear input shapers, including two-, three-impulse shaper, and robust shaper. However, these shapers are reconsidered and clarified through a more in-depth analysis with an energy perspective. We then showcase the optimal result of the generalized three-impulse shaper, where the shaper's parameter is optimized. By incorporating the energy perspective, it can be proven that the nonlinear three-impulse shaper, inspired by [19], represents the optimum case. This result can be extended to a robust nonlinear shaper and re-expressed in a compact form. Additionally, a novel nonlinear shaper called the fast-nonlinear shaper is proposed to enhance the time-delay of traditional linear and nonlinear shapers. Finally, a sensitivity issue of the proposed nonlinear input shapers to plant uncertainties is observed.

2.0 INPUT SHAPING BASICS

An example illustrating the cancellation of two impulse responses is shown in Figure 1. When an impulse input with amplitude A_1 at time t_1 is applied to a second-order linear underdamped system with a transfer function $\omega_n^2/(s^2+2\zeta\omega_n s+\omega_n^2)$, the residual vibration occurring in response (dotted line) can be eliminated by using a second impulse input with an appropriate amplitude A_2 at time t_2. Consequently, the response after this second impulse action exhibits zero residual vibration (red line).

To understand the input shaping concept, let us consider the impulse response of a single impulse input (t_1, A_1) given in Eq. (1):

$$x(t)=A_1\frac{\omega_n}{\sqrt{1-\zeta^2}}e^{-\zeta\omega_n(t-t_1)}\sin\omega_d(t-t_1),\quad t\geq t_1 \tag{1}$$

where ω_n is the undamped natural frequency and ζ is the damping ratio. The corresponding damped frequency ω_d and period T_d can be calculated by $\omega_d=\omega_n\sqrt{(1-\zeta^2)}$ and $T_d=2\pi/\omega_d$.

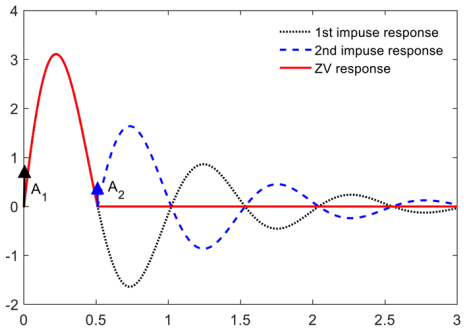

Figure 1 Cancellation of two-impulse responses.

When an N-impulse input $(t_1, A_1) + \ldots + (t_N, A_N)$ is applied to the system, the impulse response of linear system satisfies the superposition principle and is expressed as $x(t) = A_\Sigma \sin(\omega_d t - \psi),\ t \geq t_1$, where

$$A_\Sigma = \frac{\omega_n}{\sqrt{1-\zeta^2}} e^{-\zeta\omega_n(t-t_1)} \sqrt{\begin{matrix}[\Sigma_{i=1}^{N} A_i e^{\zeta\omega_n t_i} \cos(\omega_d t_i)]^2 \\ +[\Sigma_{i=1}^{N} A_i e^{\zeta\omega_n t_i} \sin(\omega_d t_i)]^2\end{matrix}} \quad (2)$$

To quantify the amount of vibration in the response, the *Percentage Residual Vibration (PRV)*, V is used as an indicator to measure the residual vibration amplitude under an input shaper compared to the residual vibration amplitude of a unit impulse response without an input shaper, i.e.,

$$V(\omega_n, \zeta) = e^{-\zeta\omega_n t_n} \sqrt{\begin{matrix}[\Sigma_{i=1}^{N} A_i e^{\zeta\omega_n t_i} \cos(\omega_d t_i)]^2 \\ +[\Sigma_{i=1}^{N} A_i e^{\zeta\omega_n t_i} \sin(\omega_d t_i)]^2\end{matrix}} \quad (3)$$

According to the requirement of zero residual vibration, the PRV constraint gives $V = 0$. In particular, to relaxing this constraint, $V_1 \leq V_0$ could be set, where V_0 is the maximum allowable residual vibration. Ensuring the total move by the shaped command is the same as the move by the unshaped command, the sum of impulse amplitudes would be equal to one, i.e., $\Sigma_{i=1}^{N} A_i = 1$.

The fastest response occurs when using a two-impulse sequence ($N = 2$), referred to as the *Zero-Vibration (ZV)* shaper, with its parameters given by

$$\begin{bmatrix} A_1 & A_2 \\ t_1 & t_2 \end{bmatrix} = \begin{bmatrix} 1/(1+K) & K/(1+K) \\ 0 & T_d/2 \end{bmatrix} \quad (4)$$

where $K = \exp\{-\zeta\pi/\sqrt{1-\zeta^2}\}$ and $T_d = 2\pi/\omega_d$.

To reduce the sensitivity of the PRV with respect to ω_n and ζ, the additional differential constraint $\partial V/\partial\omega_n = 0$ (equivalent to $\partial V/\partial\zeta = 0$) will be added. In this case the shaper will consist of three impulses, and it is called the *Zero-Vibration-and-Derivative (ZVD)* shaper:

$$\begin{bmatrix} A_1 & A_2 & A_3 \\ t_1 & t_2 & t_3 \end{bmatrix} = \begin{bmatrix} K^2/(1+K)^2 & 2K/(1+K)^2 & 1/(1+K)^2 \\ 0 & T_d/2 & T_d \end{bmatrix} \quad (5)$$

Due to the robust performance advantage of the ZVD shaper over the ZV shaper, it can be effectively employed in weakly nonlinear systems by treating the system nonlinearity as uncertainty within the tolerance of a robust shaper. However, the methodology for designing the ZV and ZVD shapers, which relies on the superposition principle, will no longer hold for systems with hard nonlinearity. In the next section, the work-energy principle in classical mechanics will be used to analyze and design various types of nonlinear shapers.

3.0 WORK-ENERGY PRINCIPLE FOR NONLINEAR SHAPER DESIGN

Consider a 2-DOF rigid-flexible system shown in Figure 2, consisting of two masses where m_1 represents the rigid-body part and m_2 for the flexible-body part, connected by Duffing's spring and nonlinear damper. The coordinates x_1 and x_2 are measured from the equilibrium positions of m_1 and m_2, respectively. Let $x = x_2 - x_1$ be the relative position between two masses. The equations of motion of the plant are given by

$$\begin{cases} m_1\ddot{x}_1 + F_0(\dot{x}_1) - F_c(\dot{x}) - F_s(x) = F(t) \\ m_2\ddot{x}_2 + F_c(\dot{x}) + F_s(x) = 0 \end{cases} \quad (6)$$

where $F_0(\dot{x}_1) = c_0\dot{x}_1$ and $F_c(\dot{x}) = c\dot{x}^3$ are the linear and nonlinear damping force, respectively. $F_s(x) = (1/2)k_1x^2 + (1/4)k_3x^4$ is the elastic force from Duffing's spring, and F is the control force.

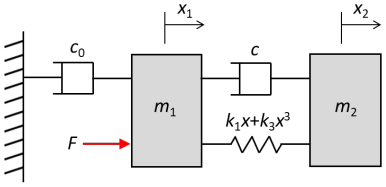

Figure 2 2-DOF rigid-flexible system with nonlinear spring and damper.

Throughout this paper, the system described in Eq. (6) will be used as the actual plant model for simulations, with the plant's parameters given by $m_1 = m_2 = 1$ kg, $k_1 = 10$ N/m, $k_3 = 100$ N/m^3, $c_0 = 0.1$ N-s/m, and $c = 0.1$ N-s^3/m^3. However, to propose closed-form solutions for the designed shapers, we will limit our scope to an undamped system ($c = 0$). This limitation will be discussed further regarding the effect of the damping coefficient. The control objective is to design a sequence of impulse signals using the energy analysis approach to generate a shaped reference input for the mass m_2, changing the system's state from a zero-initial condition state $(x_1(0), x_2(0)) = (0, 0)$ and $(\dot{x}_1(0), \dot{x}_2(0)) = (0, 0)$ to a desired final state $(x_1(t_f), x_2(t_f)) = (x_d, x_d)$ and $(\dot{x}_1(t_f), \dot{x}_2(t_f)) = (0, 0)$ with minimum residual vibration.

3.1 Nonlinear Three-Impulse Shaper

To design a three-impulse shaper (t_i, A_i), $(i = 1, 2, 3)$, consider the diagram in Figure 3. In Figure 3(a), the masses m_1 and m_2 are at rest at the equilibrium position, where the spring and damper are unstretched. To move both masses from their initial state to the final state, a first step input with a suitable amplitude A_1 is applied to the mass m_1, moving to the right (Figure 3(b)). The amplitude A_1 is pre-computed so that the mass m_2 will rest at the intermediate position $x_2 = \alpha x_d$, $(0 < \alpha \leq 1)$ at time t_2 (Figure 3(c)). As soon as mass m_2 reaches the position $x_2 = \alpha x_d$, a second step input of the appropriate amplitude A_2 is applied (Figure 3(d)), so that the mass m_2 reaches the destination $x_2 = x_d$ at time t_3 and is at rest (Figure 3(e)). At that moment, a third step input $A_3 = x_d -$

$A_1 - A_2$ should be applied to counteract the restoring force of the spring (Figure 3(f)), and both masses are at rest at $x_1 = x_2 = x_d$.

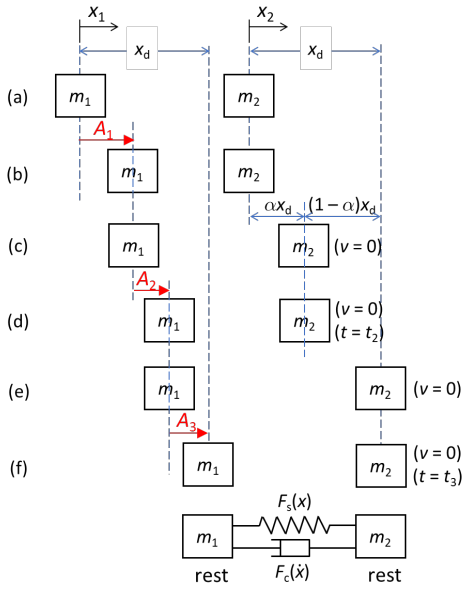

Figure 3 The schematic diagram of the nonlinear three-impulse shaper design.

With the aid of energy conservation of the mass m_2, the amplitude A_i and time location t_i of the three-impulse shaper (t_i, A_i), (i = 1, 2, 3) can be computed in the following steps:

Step 1: $0 \le x_2 \le \alpha x_d$, ($0 < \alpha \le 1$) Find the required amplitude A_1 of the first step input by considering the stages of movements from point (b) to (c) in Figure 3.

$$[T_b + U_b = T_c + U_c];\ \tfrac{1}{2}k_1(0 - A_1)^2 + \tfrac{1}{4}k_3(0 - A_1)^4 = \tfrac{1}{2}k_1(\alpha x_d - A_1)^2 + \tfrac{1}{4}k_3(\alpha x_d - A_1)^4 \quad (7)$$

$$[A_1^2 - (\alpha x_d - A_1)^2](2k_1 + k_3[A_1^2 + (\alpha x_d - A_1)^2]) = 0 \quad (8)$$

There is no solution in the second term; hence, $A_1 = \alpha x_d/2$, and assume that the first step input A_1 applies at time $t_1 = 0$. Next, to find the time t_2 of the second step input, suppose (x_2, $\dot{x}_2$) is the state of the mass m_2 at time t ($0 < t \le t_2$), where t_2 is the time taken for mass m_2 to reach $x_2 = \alpha x_d$. Applying the conservation of energy from point (b) to a general point x_2 ($0 \le x_2 \le \alpha x_d$) in Figure 3.

$$[T_b + U_b = T_{x_2} + U_{x_2}];\ \tfrac{1}{2}k_1A_1^2 + \tfrac{1}{4}k_3A_1^4 = \tfrac{1}{2}k_1(x_2 - A_1)^2 + \tfrac{1}{4}k_3(x_2 - A_1)^4 + \tfrac{1}{2}m_2\dot{x}_2^2 \quad (9)$$

Substituting $A_1 = \alpha x_d/2$, yields

$$\dot{x}_2^2 = \tfrac{1}{2m_2}(\alpha x_d - x_2)x_2[2k_1 + k_3(\tfrac{\alpha x_d^2}{2} + x_2^2 - \alpha x_d x_2)] \quad (10)$$

The time t_2 can be solved by numerical integration of $1/\dot{x}_2$ from $x_2 = 0$ to $x_2 = \alpha x_d$. However, the above expression can also be rewritten in a neater form. Without loss of generality, let us assume that $x_d > 0$, and so $\dot{x}_2 > 0$ for $0 < x_2 \le \alpha x_d$, ($0 < \alpha \le 1$). By changing the variable $y = x_2/\alpha x_d$, ($0 \le y \le 1$),

$$\dot{y}^2 = \omega^2\{y(1-y)[1 + k_r\alpha^2(\tfrac{1}{2} - y + y^2)]\} \quad (11)$$

where $\omega^2 = k_1/m_2$ and $k_r = k_3x_d^2/2k_1$. Hence,

$$t_2 = \omega^{-1}\int_0^1 \{y(1-y)[1 + k_r\alpha^2(\tfrac{1}{2} - y + y^2)]\}^{-1/2}dy \quad (12)$$

With slightly more effort, by setting the dummy integration variable, $y = \sin^2(\pi\theta/2)$, the term π/ω similar in the linear ZV shaper appeared in the expression as

$$t_2 = \tfrac{\pi}{\omega}\int_0^1 \{1 + k_r\alpha^2(\tfrac{1}{2} - \sin^2\tfrac{\pi\theta}{2} + \sin^4\tfrac{\pi\theta}{2})\}^{-1/2}d\theta \quad (13)$$

Step 2: $\alpha x_d \le x_2 \le x_d$ Now, for the amplitude A_2 of the second step input, consider the stages of movements from point (d) to (e) in Figure 3.

$$[T_d + U_d = T_e + U_e];\ \tfrac{1}{2}k_1(\alpha x_d - A_1 - A_2)^2 + \tfrac{1}{4}k_3(\alpha x_d - A_1 - A_2)^4 = \tfrac{1}{2}k_1(x_d - A_1 - A_2)^2 + \tfrac{1}{4}k_3(x_d - A_1 - A_2)^4 \quad (14)$$

$$(\alpha x_d - x_d)(\alpha x_d + x_d - 2A_1 - 2A_2) \times\left(2k_1 + k_3[(\alpha x_d - A_1 - A_2)^2 + (x_d - A_1 - A_2)^2]\right) = 0 \quad (15)$$

Because there is no solution in the first and third term, then $A_2 = (\alpha x_d + x_d - 2A_1)/2$. By substituting $A_1 = \alpha x_d/2$, it becomes $A_2 = x_d/2$, and hence $A_3 = x_d - A_1 - A_2 = (1 - \alpha)x_d/2$.

Finally, find the time t_3 required for the moving mass m_2 starting from $x_2 = \alpha x_d$ to reach the desired position $x_2 = x_d$. By considering the stages of movements from point (c) to a general point x_2 in Figure 3.

$$[T_c + U_c = T_{x_2} + U_{x_2}];\ \tfrac{1}{2}k_1(\alpha x_d - A_1 - A_2)^2 + \tfrac{1}{4}k_3(\alpha x_d - A_1 - A_2)^4 = \tfrac{1}{2}k_1(x_2 - A_1 - A_2)^2 + \tfrac{1}{4}k_3(x_2 - A_1 - A_2)^4 + \tfrac{1}{2}m_2\dot{x}_2^2 \quad (16)$$

Substituting $A_1 = \alpha x_d/2$ and $A_2 = x_d/2$, yields,

$$\dot{x}_2^2 = \omega^2\alpha^2x_d^2\underbrace{(\tfrac{x_2}{\alpha x_d} - 1)}_{:=y}[\tfrac{1}{\alpha} - 1 - \underbrace{(\tfrac{x_2}{\alpha x_d} - 1)}_{:=y}] \times\{1 + \alpha^2k_r\tfrac{\alpha^2+1}{2\alpha^2} + (\underbrace{\tfrac{x_2}{\alpha x_d} - 1}_{:=y} + 1)^2 - (\tfrac{\alpha+1}{\alpha})(\underbrace{\tfrac{x_2}{\alpha x_d} - 1}_{:=y} + 1)\}] \quad (17)$$

Clarifying the above expression by considering change of variable from $\alpha x_d \le x_2 \le x_d \Rightarrow 0 \le x_2/\alpha x_d - 1 := y \le 1/\alpha - 1$, then

$$\dot{y}^2 = \omega^2y(\tfrac{1}{\alpha} - 1 - y)\{1 + k_r\alpha^2[\tfrac{\alpha^2+1}{2\alpha^2} + (y+1)^2 - \tfrac{\alpha+1}{\alpha}(y+1)]\}. \quad (18)$$

The time t_3 can be solved by numerical integration of $1/\dot{x}_2$ from $x_2 = 0$ to $\dot{x}_2 = 1/\alpha - 1$. Hence,

$$t_3 = \omega^{-1}\int_0^{1/\alpha - 1}\{y(\tfrac{1}{\alpha} - 1 - y)[1 + k_r\alpha^2 \times(\tfrac{\alpha^2+1}{2\alpha^2} + (y+1)^2 - \tfrac{\alpha+1}{\alpha}(y+1))]\}^{-1/2}dy \quad (19)$$

Finally, setting the dummy integration variable $y := (1/\alpha - 1)\sin^2(\pi\theta/2)$ in the above expression yields a slightly simpler alternative expression

$$t_3 = \frac{\pi}{\omega}\int_0^1 \{1 + k_r(1-\alpha)^2(\tfrac{1}{2} - \sin^2\tfrac{\pi\theta}{2} + \sin^4\tfrac{\pi\theta}{2})\}^{-1/2} d\theta \quad (20)$$

It should be note that the time t_3 from Eq. (20) is the next count from t_2; therefore, the third impulse would be applied at t_2 + t_3. In summary, a general solution of the nonlinear three-impulse shaper is given by

$$\begin{bmatrix} A_i \\ t_i \end{bmatrix} = \begin{bmatrix} \alpha x_d / 2 & x_d / 2 & (1-\alpha)x_d / 2 \\ 0 & t_2 & t_2 + t_3 \end{bmatrix} \quad (21)$$

where t_2 and t_3 can be obtained by numerical calculation from Eq. (13) and Eq. (20), respectively.

Remarks:

1. The sequence of impulse signals from Eq. (21) is general form of a nonlinear three-impulse shaper, which depends on the choice of the shaper's parameter α ($0 < \alpha \le 1$) to assign the intermediate position $x_2 = \alpha x_d$ with zero velocity.

1.1 For $\alpha = 1$, the three-impulse shaper reduces to a nonlinear two-impulse shaper, i.e., $A_1 = A_2 = x_d / 2$ and

$$t_2 = \frac{\pi}{\omega}\int_0^1 \{1 + k_r(\tfrac{1}{2} - \sin^2\tfrac{\pi\theta}{2} + \sin^4\tfrac{\pi\theta}{2})\}^{-1/2} d\theta \,. \quad (22)$$

1.2 For $\alpha = 1$ and $k_r = 0$ (linear spring), the nonlinear two-impulse shaper becomes the linear ZV shaper, i.e., $A_1 = A_2 = x_d / 2$ and

$$t_2 = (\pi / \omega)\int_0^1 d\theta = \pi / \omega \,. \quad (23)$$

2. The time t_2 in Eq. (13) represents the haft-period of nonlinear oscillation. Here, note that t_3 is not necessarily equal to that of t_2. However, by minimizing the residual total energy, it can be shown in the next subsection that $\alpha = 0.50$ is optimum, and so for this case, $t_2 = t_3$.

3.1.1 Optimal Parameter α and Sensitivity Consideration

Infinitely many solutions of the nonlinear three-impulse shaper in Eq. (21) depend on the selection of α. It was found that a change in the parameter α will also affect the magnitudes of A_1 and A_3 in opposite directions. When $\alpha >> 0$ or A_1 is large, then A_3 will be small (and vice versa if $\alpha \to 0$ or A_1 is small, A_3 will be large). Note that A_2 will always have a constant magnitude regardless of any choice of α value. To demonstrate the results of changes in the parameter α, consider the residual total energy, which is defined as the kinetic and elastic potential energy of the mass m_2 throughout the entire range of motion as follows,

Kinetic energy:

$$(0 \le x_2 \le \alpha x_d);\quad T_1(x_2) = \tfrac{1}{4}(\alpha x_d - x_2)x_2 \times[2k_1 + k_3(\frac{\alpha^2 x_d^2}{4} + (x_2 - \frac{\alpha x_d}{2})^2)] \quad (24)$$

$$(\alpha x_d \le x_2 \le x_d);\quad T_2(x_2) = \tfrac{1}{2}(\alpha x_d - x_2)(x_2 - x_d) \times\{k_1 + \frac{k_3}{2}[(\frac{(\alpha-1)^2 x_d^2}{4}) + (x_2 - \frac{(1+\alpha)x_d}{2})^2]\} \quad (25)$$

Potential energy:

$$(0 \le x_2 \le \alpha x_d);\quad U_1(x_2) = \tfrac{1}{2}k_1(x_2 - A_1)^2 + \tfrac{1}{4}k_3(x_2 - A_1)^4 \quad (26)$$

$$(\alpha x_d \le x_2 \le x_d);\quad U_2(x_2) = \tfrac{1}{2}k_1(x_2 - A_1 - A_2)^2 + \tfrac{1}{4}k_3(x_2 - A_1 - A_2)^4 \quad (27)$$

In simulation, let's assume the desired target position is x_d = 1 m, and the impulse sequence (t_i, A_i), (i = 1, 2, 3), corresponding to α = 0.45, 0.50, 0.55, and 1.00, can be computed from Eq. (13)-(21) and is provided in Table 1.

Table 1 Design parameters for a general solution of nonlinear three-impulse shaper at each α.

α	(t_1, A_1)	(t_2, A_2)	(t_3, A_3)
0.45	(0, 0.225)	(0.847, 0.500)	(1.643, 0.275)
0.50	(0, 0.250)	(0.822, 0.500)	(1.643, 0.250)
0.55	(0, 0.275)	(0.796, 0.500)	(1.643, 0.225)
1.00	(0, 0.500)	(0.591, 0.500)	-

Figure 4 compares the profiles of residual total energy of the nonlinear three-impulse shaper for any choice of α. It can be seen that the residual total energy of the system at each α is not equal. When α = 1.00 (two-impulse shaper) the system generates maximum energy. However, it is important to note that the total energy of the system is conserved when α = 0.50 and α = 1.00. For this case, the potential energy function is a continuous function, which has "no jump" in the profiles. As a result, the spring force does not undergo an abrupt change during the second impulse.

To eliminate such discontinuities, the best approach is to equalize $U_1(x_2)$ and $U_2(x_2)$ at the second impulse or at the switching points $x_2 = \alpha x_d$, so that neither the intermediate nor the desired positions are more sensitive to timing errors. This statement is equivalent to the work done by the spring force from the first impulse being equal to that of the second impulse. In other words, it should consider the balance of restoring spring force f_c at the stages in Figure 3(c) and f_e in Figure 3(e), where $f_c = k_1\alpha x_d/2 + k_3(\alpha x_d)^3/8$ and $f_e = k_1(1 - \alpha x_d/2 + k_3((1 - \alpha)x_d)^3/8$. Accordingly, the "optimal" value of the parameter α_{opt} can be calculated from the algebraic equation:

$$[f_c = f_e];\quad 1 - 2\alpha_{opt} + \frac{k_r}{2}(1 - 3\alpha_{opt} + 3\alpha_{opt}^2 - 2\alpha_{opt}^3) = 0 \quad (28)$$

where $k_r = k_3 x_d^2 / 2k_1$. Eq. (28) has a unique solution α_{opt} = 0.50. Consequently, the *optimal (α_{opt} = 0.50) nonlinear three-impulse shaper* can be expressed as

$$\begin{bmatrix} A_1 & A_2 & A_3 \\ t_1 & t_2 & t_3 \end{bmatrix} = \begin{bmatrix} x_d / 4 & x_d / 2 & x_d / 4 \\ 0 & t_2 & t_2 + t_3 \end{bmatrix} \quad (29)$$

where the action time t_2 and t_3 can then be obtained from Eq. (13) and Eq. (20), as follows

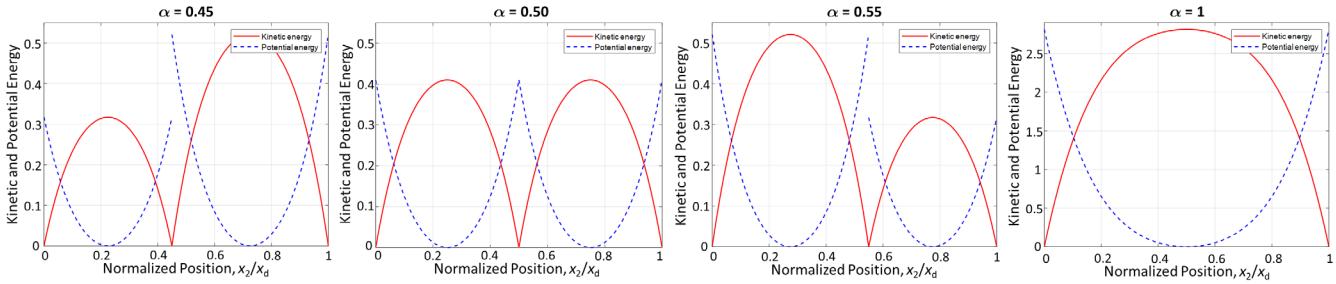

Figure 4 Residual energy profiles when using a general nonlinear three-impulse shaper.

$$\begin{cases} t_2 = \omega^{-1}\int_0^1 \{y(1-y)[1+\frac{k_r}{4}(\frac{1}{2}-y+y^2)]\}^{-1/2}\,dy \\ t_3 = t_2 \end{cases} \tag{30}$$

In this case, to verify the optimality of the shaper parameter α_{opt} = 0.50, sensitivity curves are employed, plotting the percentage residual vibration (PRV (%)) against the normalized plant's parameter of interest. While typical sensitivity curves of linear input shapers can reflect tolerance to errors in estimating the system's natural frequency and damping ratio, they are unsuitable for highly nonlinear situations due to variable-dependent natural frequencies and damping ratios that cannot be easily defined. In this instance, PRV (%) is measured using the criteria from [18]: PRV (%) = $(x_p - x_d)/x_d$, where x_p is the first maximum overshoot, and x_d is the desired position of movement. Figure 5, shows the sensitivity curves with respect to the normalized mass m_{2a}/m_{2m}, varying the parameter α of the nonlinear three-impulse shaper from α = 0.50 to 0.70. The simulation confirms that overall residual vibration is minimized when using α_{opt} = 0.50; hence, this optimum value will be used in the design of the robust nonlinear shaper in the next section.

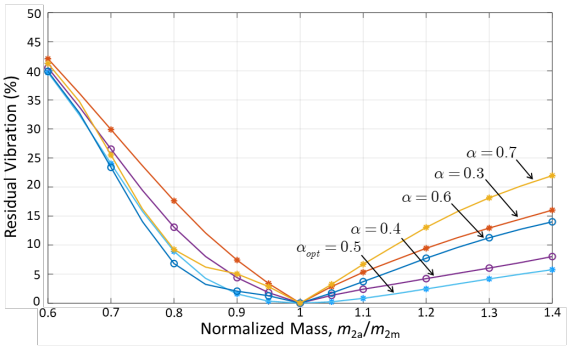

Figure 5 Effect of the shaper's parameter α on percentage residual vibration.

3.2 Robust Nonlinear Shaper

Due to the resting point of the mass m_2 in the optimal nonlinear three-impulse shaper being designed as one resting point during the motion at $x_d/2$, to cope with the uncertainty in the plant model, a robust nonlinear shaper can be developed using the same concept. This involves adding k-resting points (k = 0, 1, …) for the mass m_2 before reaching the desired position $x = x_d$. With this setting, when k = 0, it means that there is no stationary point during the motion; for k = 1, it represents the foregoing optimal nonlinear three-impulse shaper. As a result, the distance during each step is equal to $x_d/(k+1)$, taking up half-period of oscillation either in linear or nonlinear oscillation.

Let A_1, A_2, …, A_{k+2} be the amplitudes of the impulse signals acting at times t_1, t_2, …, t_{k+2}, respectively. The mass m_2 is stimulated by the first impulse from the zero-initial state ($x_2(0)$, $\dot{x}_2(0)$) = (0, 0) to the resting point $x_2 = x_d/(k+1)$. Then the subsequent impulse signals (t_i, A_i), (I = 2, 3), are stimulated at times $t_2 = T/2$, $t_3 = T$, $t_4 = 3T/2$, …, $t_{k+2} = (k+1)T/2$, where T is the haft-period of oscillation, until the mass m_2 moves to the desired position $x_2 = x_d$. The final impulse (t_{k+2}, A_{k+2}), where $A_{k+2} = A_1$, is applied to counteract the excess potential energy generated by the previous impulse, so the system is at rest at the destination $x_2 = x_d$.

Finding the sequence of impulse signals is, therefore, simply finding the first amplitude A_1, which is the same as the final amplitude A_{k+2}, and the amplitude $A_2 = A_3 = \ldots = A_{k+1}$ used during the movement, as follows,

$$\begin{cases} A_1 = A_{k+2} = \dfrac{x_d}{2(k+1)} \\ A_i = \dfrac{x_d}{k+1},\ i = 2, 3, \ldots, k+1 \end{cases} \tag{31}$$

The half-period time $T/2$ can be determined from the first movement stage, from $x_2 = 0$ to $x_2 = x_d/(k+1)$, using the conservation of energy. This result can be applied in subsequent periods.

$$\frac{1}{2}k_1A_1^2 + \frac{1}{4}k_3A_1^4 = \frac{1}{2}k_1(x_2 - A_1)^2 + \frac{1}{4}k_3(x_2 - A_1)^4 + \frac{1}{2}m_2\dot{x}_2^2 \tag{32}$$

Substituting $A_1 = x_d/2(k+1)$, yields

$$\dot{x}_2^2 = \omega^2 x_d^2\left(\frac{1}{k+1} - \frac{x_2}{x_d}\right)\frac{x_2}{x_d}\left\{1 + k_r\left[\frac{1}{4(k+1)^2} + \left(\frac{x_2}{x_d} - \frac{1}{2(k+1)}\right)^2\right]\right\} \tag{33}$$

As in the same process before, because $0 \le x_2 \le x_d/(k+1) \Rightarrow 0 \le (k+1)x_2/x_d := y \le 1$, the above equation becomes,

$$\dot{y}^2 = \omega^2\{y(1-y)[1 + \frac{k_r}{(k+1)^2}(\frac{1}{2} - y + y^2)]\} \tag{34}$$

Hence,

$$t_2 = \omega^{-1}\int_0^1 \{y(1-y)[1 + \frac{k_r}{(k+1)^2}(\frac{1}{2} - y + y^2)]\}^{-1/2}\,dy \tag{35}$$

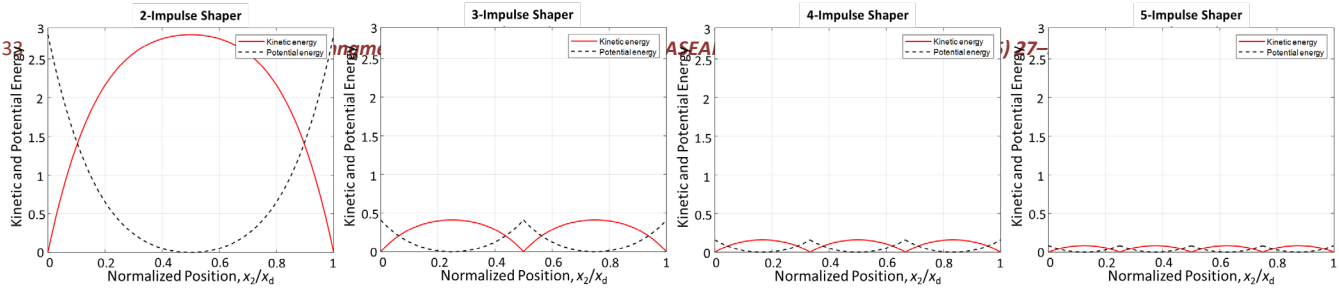

Figure 6 Residual energy profiles of the robust nonlinear shapers for k = 0 (non-robust), 1, 2, and 3.

By changing of variable $y = \sin^2(\pi\theta/2)$, the haft-period time used is

$$t_2 = \frac{T}{2} = \frac{\pi}{\omega}\int_0^1 \{1 + \frac{k_r}{(k+1)^2}(\frac{1}{2} - \sin^2\frac{\pi\theta}{2} + \sin^4\frac{\pi\theta}{2})\}^{-1/2}\, d\theta \qquad (36)$$

In summary, the robust nonlinear shaper with k + 2 impulses, where k = 0, 1, … is given by

$$\begin{bmatrix} A_i \\ t_i \end{bmatrix} = \begin{bmatrix} A & A/2 & A/2 & \cdots & A/2 & A \\ 0 & T/2 & T & \cdots & kT/2 & (k+1)T/2 \end{bmatrix} \qquad (37)$$

where i = 1, 2, …, k + 2, $A = x_d/(k+1)$ and T is a period of oscillation given in Eq. (36).

Remarks:

1. For a special case where $k_r \neq 0$ and k = 0, the robust nonlinear shaper reduces to a nonlinear two-impulse shaper, and a nonlinear three-impulse shaper when k = 1.
2. For a large number of k-impulses, the half-period of oscillation has a smaller corresponding to small displacements. Theoretically, if $k \to \infty$, then $t_2 \to \pi/\omega$, which is equal to half-period of simple harmonic. That is, a linear ZVD^k can be used with large k values for two-mass systems with nonlinear springs.
3. From energy perspective, using a large number of k-impulses in a robust nonlinear shaper corresponds to a decrease in the residual total energy, as shown in Figure 6. It can be seen that the maximum residual energy occurs for k = 0 (two impulses). When k = 1 (three impulses), the residual total energy was reduced by 6.7 times, 2.6 times compared to before, and 1.9 times when using k = 2 (four impulses) and k = 3 (five impulses), respectively. However, for any k-impulses, the residual total energy of the system remains consistent throughout the motion (conserved system).

3.3 Fast Three-Impulse Shaper

The rise time of system response with the traditional linear shaper (ex. ZVD^k), and the aforementioned nonlinear shapers depends on the number of impulses in the shaper. In general, more impulses can be added to the sequence to increase robustness but expense of longer moving time. This is because the design of most shapers is based on the concept of half-cycle or half-period delay condition. To improve such time delay in the response, a novel nonlinear shaper called the *fast three-impulse shaper* is proposed in such a way that the second impulse stimulates when the flexible-part of flexible system reaches its maximum velocity (corresponding to maximum kinetic energy). As a result, the delay time is reduced to a quarter of the period, and not only is the rise time of the response reduced compared to the two-impulse shaper, but it also improves the robust performance to the plant's uncertainties. This issue will be discussed further in the section of sensitivity analysis.

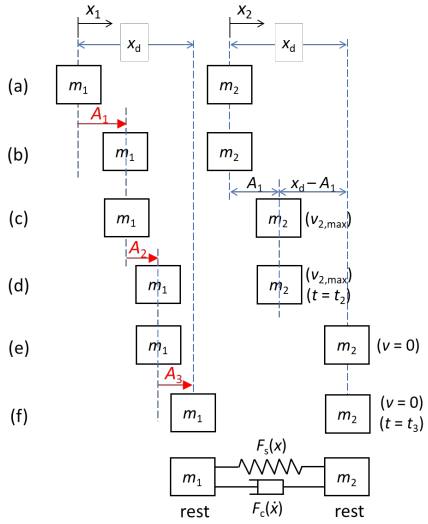

Figure 7 The schematic diagram of the fast three-impulse shaper design.

Step 1: $0 \le x_2 \le A_1$ The amplitudes A_1 stimulates mass m_1, such that the moving mass m_2 reaches its maximum velocity $v_{2,\max}$ at $x_2 = A_1$ (equilibrium position). It can be immediately known that the relation between A_1 and $v_{2,\max}$ changes in the same direction. To evaluate $v_{2,\max}$, consider the conservation of energy from point (b) to (c) in Figure 7, yielding

$$[T_b + U_b = T_c + U_c]; \quad \tfrac{1}{2}k_1A_1^2 + \tfrac{1}{4}k_3A_1^4 = \tfrac{1}{2}m_2v_{2,\max}^2 \qquad (38)$$

$$v_{2,\max}^2 = \frac{k_1}{m_2}A_1^2 + \frac{k_3}{2m_2}A_1^4 \qquad (39)$$

Let t_2 be the time taken for mass m_2 to travel from x_2 = 0 to $x_2 = A_1$. To calculate t_2, apply the conservation of energy from point (b) to a general point x_2 ($0 \le x_2 \le A_1$) in Figure 7.

$$[T_b + U_b = T_{x_2} + U_{x_2}]; \quad \tfrac{1}{2}k_1A_1^2 + \tfrac{1}{4}k_3A_1^4 = \tfrac{1}{2}k_1(x_2 - A_1)^2 + \tfrac{1}{4}k_3(x_2 - A_1)^4 + \tfrac{1}{2}m_2\dot{x}_2^2 \qquad (40)$$

Then,

$$\dot{x}_2^2 = \omega^2\{A_1^2 - (x_2 - A_1)^2 + \frac{k_3}{2k_1}[A_1^4 - (x_2 - A_1)^4]\} \qquad (41)$$

This works similar in the step to find t_2 for the design of nonlinear three-impulse shaper. Suppose $A_1 > 0$, and so $\dot{x}_2 > 0$. For $0 \le x_2 \le A_1$, by changing the variable $y = x_2/A_1$, ($0 \le y \le 1$), this yields

$$\dot{y}^2 = \omega^2\{1-(y-1)^2[1+\frac{k_3A_1^2}{2k_1}(1+(y-1)^2)]\} \quad (42)$$

Hence,

$$t_2 = \omega^{-1}\int_0^1 \{1-(y-1)^2[1+\frac{k_3A_1^2}{2k_1}(1+(y-1)^2)]\}^{-1/2}\,dy \quad (43)$$

Step 2: $A_1 \le x_2 \le x_d - A_1$ As soon as mass m_2 reaches the position $x_2 = A_1$ with maximum velocity, the second impulse with amplitude A_2 should be applied to move m_2 to the destination with zero velocity. To find A_2, consider the stages of movements from point (d) to (e) in Figure 7, yielding

$$\tfrac{1}{2}m_2v_{2,\max}^2 + \tfrac{1}{2}k_1(A_1-A_1-A_2)^2 + \tfrac{1}{4}k_3(A_1-A_1-A_2)^4 = \tfrac{1}{2}k_1(x_d-A_1-A_2)^2 + \tfrac{1}{4}k_3(x_d-A_1-A_2)^4 \quad (44)$$

Substituting $v_{2,\max}$ and rearranging the equation, yields

$$A_1^2 + A_2^2 - (x_d-A_1-A_2)^2 + \frac{k_3}{2k_1}\left[A_1^4 + A_2^4 - (x_d-A_1-A_2)^4\right] = 0 \quad (45)$$

Eq. (45) can be rewritten in dimensionless form by introducing $x = A_1/x_d$ and $y = A_2/x_d$, hence

$$x^2 + y^2 - (1-x-y)^2 + k_r\left[x^4 + y^4 - (1-x-y)^4\right] = 0 \quad (46)$$

For this case, the amplitudes A_1 and A_2 (also A_3) in Eq. (45) (corresponding to x, y, and z in Eq. (46)) are expressed through the implicit relations, as shown in Figure 8 (dashed line for nonlinear case). These relations cannot be explicitly solved in closed-form solutions, rendering them unsuitable for practical use. However, the optimal amplitude solutions can be further obtained with an energy perspective.

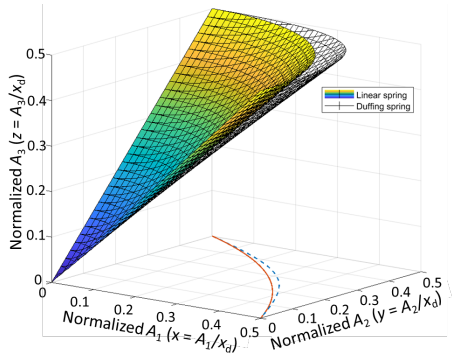

Figure 8 Relationship between normalized amplitudes A_1, A_2 (left) and A_1, A_2, A_3 (right) of the fast three-impulse shaper.

Step 3: $A_1 \le x_2 \le x_d$ When the mass m_2 reaches the desired position $x_2 = x_d$, the final impulse with amplitude A_3 should be applied at time t_3. To find time t_3, consider the stages of movements from point (d) to a general point x_2 in Figure 7.

$$[T_c + U_c = T_{x_2} + U_{x_2}];\ \tfrac{1}{2}m_2v_{2,\max}^2 + \tfrac{1}{2}k_1(A_1-A_1-A_2)^2 + \tfrac{1}{4}k_3(A_1-A_1-A_2)^4 = \tfrac{1}{2}k_1(x_2-A_1-A_2)^2 + \tfrac{1}{4}k_3(x_2-A_1-A_2)^4 + \tfrac{1}{2}m_2\dot{x}_2^2 \quad (47)$$

Substituting $v_{2,\max}$ yields,

$$\dot{x}_2^2 = \frac{k_1(x_d-A_1)^2}{m_2}\left\{\frac{A_1^2}{(x_d-A_1)^2} + \frac{A_2^2}{(x_d-A_1)^2} - \left(\frac{x_2-A_1}{x_d-A_1} - \frac{A_2}{x_d-A_1}\right)^2 + \frac{k_3(x_d-A_1)^2}{2k_1}\left[\frac{A_1^4}{(x_d-A_1)^4} + \frac{A_2^4}{(x_d-A_1)^4} - \left(\frac{x_2-A_1}{x_d-A_1} - \frac{A_2}{x_d-A_1}\right)^4\right]\right\} \quad (48)$$

By change of variable from $A_1 \le x_2 \le x_d \Rightarrow 0 \le (x_2 - A_1)/(x_d - A_1) := y \le 1$, the above expression becomes,

$$\dot{y}^2 = \omega^2\{c_1^2 + (c_2^2 - (y-c_2)^2)[1+K_r(c_2^2+(y-c_2)^2)]\} \quad (49)$$

Hence,

$$t_3 = \omega^{-1}\int_0^1 \{c_1^2 + (c_2^2-(y-c_2)^2)[1+K_r(c_2^2+(y-c_2)^2)]\}^{-1/2}\,dy \quad (50)$$

where $c_1 = [A_1/(x_d-A_1)]\sqrt{1+k_3A_1^2/2k_1}$, $c_2 = A_2/(x_d-A_1)$, and $K_r = k_3(x_d-A_1)^2/2k_1$.

In summary, the time locations for the fast three-impulse shaper can be computed using symbolic integration Eq. (43) for t_2 and Eq. (50) for t_3.

3.3.1 Energy Perspective on Fast Three-Impulse Shaper

Due to the second impulse of the fast three-impulse shaper acting when the mass m_2 reaches its maximum velocity (corresponding to maximum kinetic energy), the total energy of m_2 increases from the previous maximum kinetic energy. The additional energy comes from the potential energy exerted by the second impulse. Therefore, the total energy over the entire range of motion is not consistent (not a conservative system), which is not the same as for the three-impulse shaper or robust shaper. Additionally, it can be seen that a "jump" in the potential energy curve occurs at the second impulse (see Figure 9). This does not happen in the case of three-impulse shaper or robust shaper, where the potential energy curve is a continuous function. Consequently, it can be expected that the time-delay will be decreased, while a higher timing error occurs compared to that of the three-impulse shaper and robust shaper, affecting the sensitivity to parameters uncertainty.

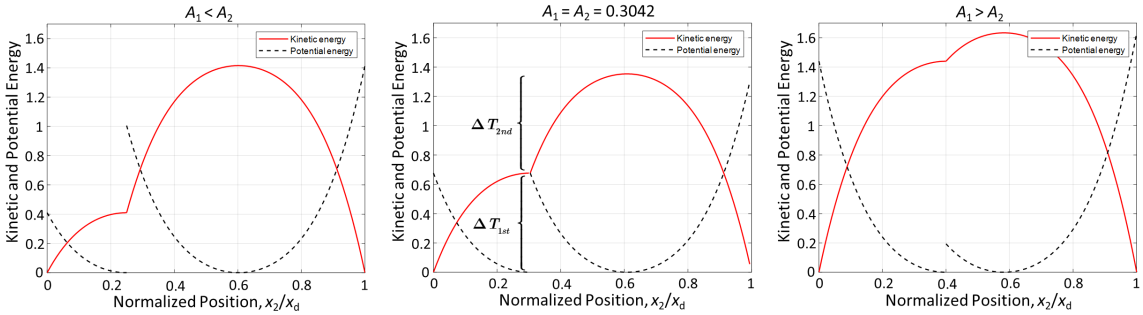

Figure 9 Residual energy profiles of the fast three-impulse shaper for $A_1 < A_2$, $A_1 = A_2$, and $A_1 > A_2$, respectively

To clarity, let us consider the energy profiles shown in Figure 9, comparing different sets of impulse signals determined from the amplitude, which is related according to Eq. (45). When $A_1 < A_2$ (in this case, $A_1 = 0.25$, $A_2 = 0.3523$), the potential energy increase from the second impulse is greater than the previous maximum kinetic energy from the first impulse, and vice versa for $A_1 > A_2$ (here, $A_1 = 0.40$, $A_2 = 0.1823$). However, when $A_1 = A_2$ (in this case, $A_1 = A_2 = 0.3042$), it can be seen that the second impulse's potential energy is equal to the first impulse's kinetic energy. It should be noted that due to the second impulse acting when the mass m_2 reaches its maximum kinetic energy, the total energy during the second impulse will suddenly increase ("jump") from the previous maximum kinetic energy and always be greater than the total energy during the first impulse. The additional energy comes from the potential energy exerted by the second impulse while the kinetic energy is not zero.

To evaluate suitable amplitudes A_1, A_2 (also A_3), perhaps the best approach is to equalize the work done by the first impulse and second impulses. The result is that the first and second impulses cause the same change in kinetic energy ($\Delta T_{1st} = \Delta T_{2nd}$).

Consider $\dot{x}_2^2$ from Eq. (41) for $0 \le x_2 \le A_1$, and from Eq. (48) for $A_1 \le x_2 \le x_d$. It can be obtained,

Kinetic energy:

$$(0 \le x_2 \le A_1);\quad T_1(x_2) = \frac{k_1}{2}\{A_1^2 - (x_2 - A_1)^2 + \frac{k_3}{2k_1}[A_1^4 - (x_2 - A_1)^4]\} \tag{51}$$

$$(A_1 \le x_2 \le x_d);\quad T_2(x_2) = \frac{k_1}{2}\{A_1^2 + A_2^2 - (x_2 - A_1 - A_2)^2 + \frac{k_3}{2k_1}[A_1^4 + A_2^4 - (x_2 - A_1 - A_2)^4]\} \tag{52}$$

Potential energy:

$$(0 \le x_2 \le A_1);\quad U_1(x_2) = \frac{k_1}{2}(x_2 - A_1)^2 + \frac{k_3}{4}(x_2 - A_1)^4 \tag{53}$$

$$(A_1 \le x_2 \le x_d);\quad U_2(x) = \frac{k_1}{2}(x_2 - A_1 - A_2)^2 + \frac{k_3}{4}(x_2 - A_1 - A_2)^4 \tag{54}$$

Setting $T_{1,\max}(x_2) = U_2(x_2)$ at $x_2 = A_1$, then $(k_1/2)A_1^2 + (k_3/4)A_1^4 = (k_1/2)A_2^2 + (k_3/4)A_2^4$. The unique condition would then be $A_1 = A_2$ (corresponding to $x = y$). By substituting this into Eq. (45) (or Eq. (46)), the optimal solution can be obtained as $x = y = 0.3042$ and $z = 1 - x - y = 0.3916$ (corresponding to $A_1 = A_2 = 0.3042x_d$ and $A_3 = x_d - A_1 - A_2 = 0.3916x_d$).

To verify the transient performance of all proposed nonlinear input shapers, a linear ZVD shaper was used to compare the speed of responses in terms of rise-time. The shapers' parameters are designed and given in Table 2.

Table 2 Amplitudes and time locations of the designed shapers.

Shapers	Impulse sequences (t_i, A_i)
Linear ZVD (3-impulse)	(0, 0.25), (0.994, 0.50), (1.987, 0.25)
2-impulse	(0, 0.50), (0.591, 0.50)
3-impulse	(0, 0.25), (0.822, 0.50), (1.643, 0.25)
4-impulse	(0, 0.167), (0.904, 0.333), (1.809, 0.333), (2.713, 0.167)
Fast 3-impulse	(0,0.3042), (0.383, 0.3042), (0.926, 0.392)

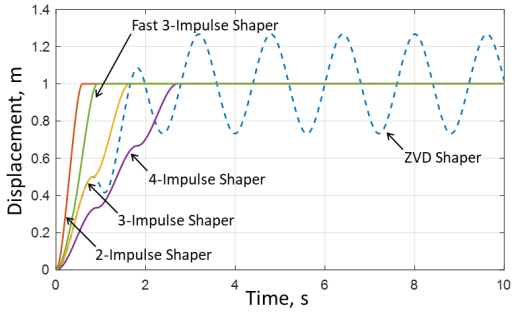

Figure 10 Time response comparison between designed nonlinear shapers and ZVD linear shaper.

Figure 10 shows the system responses of the position of mass m_2, where given the desired target position x_d = 1m. For this case, the perfect plant model was considered. Although the linear ZVD shaper was designed to accommodate plant parameter uncertainties, it cannot eliminate residual vibration in the system with Duffing nonlinearity. The rise time for the two-impulse and fast three-impulse are quite similar, while the robust nonlinear shapers will provide slower responses when using a higher impulse number.

4.0 ROBUST PERFORMANCE OF THE DESIGNED NONLINEAR INPUT SHAPERS

In summary, the energy analysis approach not only provides a clearer way to understand nonlinear input shaping but also

offers a more comprehensive methodology for design that can be used in both linear and nonlinear systems. From the aforementioned designed nonlinear input shapers, the amplitudes A_i and times t_i of all the proposed shapers can be concluded in the same expression of a general form as follows,

$$\begin{cases} A_i = A(x_d, k) \\ t_i = \omega(k_1, m_2)\int_0^1 h(k_1, k_3)\,dy \end{cases} \quad (55)$$

where $A(x_d, k)$ is the amplitude function, which depends on the desired final position x_d, and the number of impulses k (for the robust shaper case). The time location t_i is a function of m_2, k_1, and k_3, defined as the function ω multiplied by the integral from 0 to 1 of the integrand h.

This is useful for analyzing the robust performance of the designed shapers. Since the actual plant's parameters can differ from the design value by various reasons, such as aging of mechanical elements and stress relaxation, etc., this issue will be discussed in the next section by cooperating with Eq. (55).

4.1 Sensitivity Analysis Against Plant's Parameters Variations

To compare robust performance of the designed shapers, the PRV (%) will be used to show the effectiveness of residual vibration elimination by plotting with respect to the modeling errors, including the normalized mass m_{2a}/m_{2m}, the normalized spring's stiffnesses k_{1a}/k_{1m}, and k_{3a}/k_{3m}.

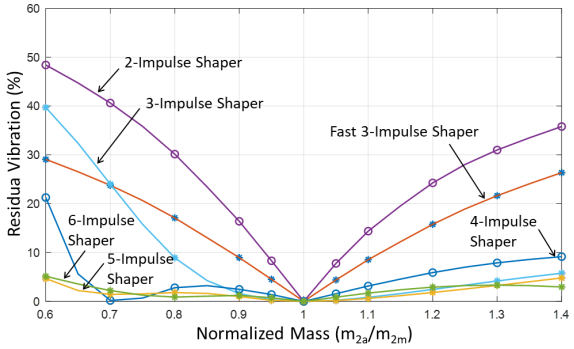

Figure 11 Percentage residual vibration vs. normalized mass m_{2a}/m_{2m}.

Figure 11 summarizes the sensitivity curves subject to m_{2a}/m_{2m}. It can be seen that the two-impulse shaper and fast three-impulse shaper are quite inferior to the robust shapers (three impulses or more) in terms of robustness. However, the fast three-impulse shaper is more robust than the two-impulse shaper because the added impulse can compensate the effect of timing errors that occur when the shaper switches. For the robust shapers with k+2 impulses, using a larger number of impulses does not guarantee robust performance at every m_{2a}/m_{2m}, as seen in the four-impulse shaper at m_{2a}/m_{2m} = 0.6. This is because when the impulse signal is applied, there will always be errors in the time locations calculation from Eq. (55) . This error arises from the term ω and accumulates with the number of impulses applied. Nevertheless, increasing the number impulses will reduce the overall residual total energy to compensate for errors in time locations calculation. It was found that for the four-impulse shaper, the maximum PRV is 22% at m_{2a}/m_{2m} = 0.6, and less than 5% when using five-impulse and six-impulse shapers.

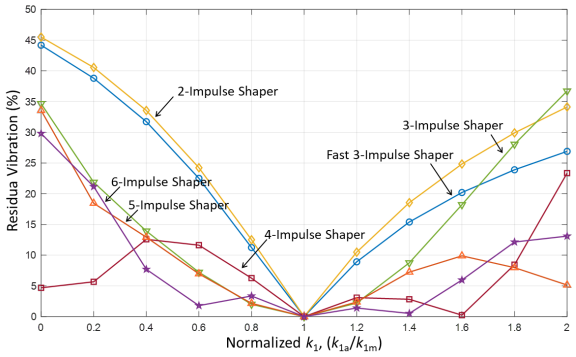

Figure 12 Percentage residual vibration vs. normalized spring's stiffness k_{1a}/k_{1m}.

Figure 12 illustrates the sensitivity curves concerning k_{1a}/k_{1m}. The robustness of the two-impulse shaper closely resembles that of the fast three-impulse shaper, similar to the plotting with m_{2a}/m_{2m}. However, inconsistent results emerge for robust shapers (three impulses or more). Despite using a higher number of impulses in robust shapers, the robustness of the shapers, when compared at the same value of k_{1a}/k_{1m}, does not necessarily increase with the number of impulses used. This discrepancy arises because, from Eq. (55), variations of k_1 from a nominal design value affect both functions ω and h, exerting a greater influence on time locations calculations than variations in parameters m_2 and k_3 (compare with Figure 11 and Figure 13). Nevertheless, the impact of increasing the number of impulses, resulting in decreased residual total energy, outweighs the effect of errors from time location calculations. This is evident from an overview that robust shapers are more robust than two-impulse and fast three-impulse shapers.

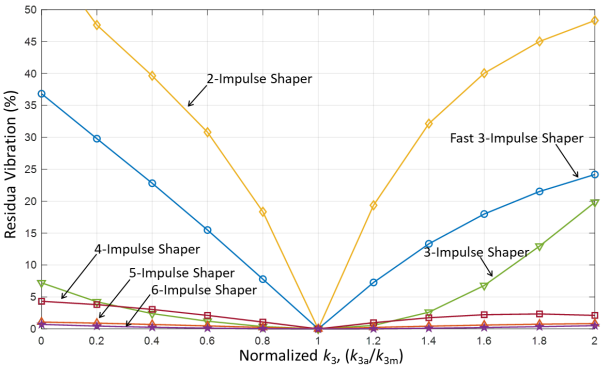

Figure 13 Percentage residual vibration vs. normalized spring stiffness k_{3a}/k_{3m}.

Figure 13 compares the sensitivity curves with respect to k_{3a}/k_{3m}. By cooperating with Eq. (55), the parameter k_3 affects the time calculation only in the term of integrand h. Therefore, errors in the time location calculations would be less than k_1, which appears in the multiplied functions ω and h. As a result, the change in residual vibration in this case is similar to the case of the normalized mass m_{2a}/m_{2m}. However, the robustness of the fast three-impulse shaper is significantly better than that of the two-impulse shaper by approximately 50%, considering the same value of k_{3a}/k_{3m} (and also in m_{2a}/m_{2m}).

4.2 The Effect of Damping Coefficient

The nonlinear damping force $F_c(\dot{x}) = c\dot{x}^3$ was ignored in the procedure of designing nonlinear shapers in order to obtain a closed-form solutions. However, it is inevitable for damped flexible systems, as the damping force can degrade the shaper's performance due to inaccurate time calculations for the impulse signals. The impact of the damping force depends on the number of impulses used, which dissipates the system's kinetic energy. For instance, when using an input shaper with a large number of impulses, a slower response affects the kinetic energy dissipation less than the shaper with a small number of impulses, which is faster.

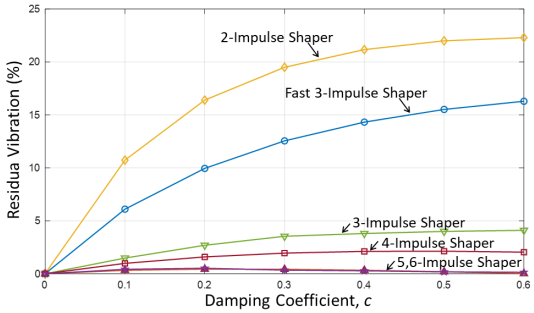

Figure 14 Impact of damping coefficient on percentage residual vibration.

Figure 14 depicts the impact of damping coefficient on the percentage residual vibration. Nonlinear damping forces most affect the response when using the two-impulse shaper, followed by the fast 3-impulse shaper, where the PRV (%) was as high as 23% and 17% at c = 0.6 N-s^3/m^3, respectively. In contrast, the robust shaper (three impulses or more) exhibits higher damping tolerance, with PRV (%) not exceeding 5% over the range of c. In fact, the influence of the F_c increases with the speed of response, the slower responses of the robust shapers resulting in a more minimal impact of the nonlinear damping force. Furthermore, it is observed that the PRV (%) initially increases with the increase of c. Subsequently, it remains relatively constant as the damping in the system further increases, ultimately leading to no vibration. However, this is not a problem in designing robust nonlinear shapers (with k+2 impulses) for real systems with damping, as the damping force can be combined within the system dynamics to calculate the half-period time of the oscillation for any k impulses, rather than relying on Eq. (36).

5.0 CONCLUSIONS

This study revisited and clarified a comprehensive framework for designing nonlinear input shapers, including the three-impulse shaper, robust shaper, and a novel fast three-impulse shaper. The versatility and effectiveness of the proposed shapers were demonstrated through the displacement excitation of a 2-DOF flexible system with Duffing nonlinearity. The first proposed shaper, a general three-impulse shaper, is optimized by minimizing residual total energy, resulting in the optimal three-impulse shaper. This result is extended to the robust shaper with k+2 impulses, covering special cases of nonlinear two- and three-impulse, as well as linear ZV and ZVD shapers. Energy analysis revealed that increased robustness in robust shapers with more impulses is attributed to decreased residual total energy. The fast three-impulse shaper, designed to improve rise time, exhibited better robustness than the two-impulse shaper but introduced timing errors, mitigable by specific impulse settings. The general solution of all the shaper amplitudes and time locations can be expressed in a uniform format suitable for analyzing the robust performances. The augmentation of impulse numbers in robust shapers affects robustness differently, depending on the uncertain parameters. Nonetheless, robust shapers demonstrated superior robustness, with the impact of decreased residual total energy outweighing errors in time calculations. Finally, the nonlinear damping effect was discussed, emphasizing that the designing a robust shaper with k+2 impulses for the damped system case can be accomplished by including the damping force in the plant dynamics, followed by numerical calculation for the haft-period of movements depending on the number of impulses used. Additionally, with the same energy concept in the proposed shaper design, it can be applied to real-life applications with 2-DOF, such as flexible-joint robots, trolley-pendulum system, and gantry crane. By applying the conservation of energy to any type of motion (translation and/or rotation) [12], depending on each system, the shaper design process remains consistent.

Future work will involve applying the proposed approach to other general nonlinear systems and extending it to multi-input-multi-output systems, such as bridge cranes, to enhance its applicability and effectiveness in more complex scenarios.

Acknowledgement

The authors would like to extend their gratitude to the Control of Robot and Vibration Laboratory, Department of Mechanical Engineering, Faculty of Engineering, at the Kasetsart University, and all who have contributed to the success of this study.

Conflicts of Interest

The author(s) declare(s) that there is no conflict of interest regarding the publication of this paper

References

[1] Montonen, J. H., Nevaranta, N., Niemelä, M., & Lindh, T. 2022. Comparison of extrainsensitive input shaping and swing-angle-estimation-based slew control approaches for a tower crane. *Applied Sciences*. 12(12): 5945. DOI: https://doi.org/10.3390/app12125945

[2] Thomsen, D. K., Søe-Knudsen, R., Balling, O., & Zhang, X. 2021. Vibration control of industrial robot arms by multi-mode time-varying input shaping. *Mechanism and Machine Theory*. 155: 104072. DOI: https://doi.org/10.1016/j.mechmachtheory.2020.104072

[3] Wang, W., Hu, C., Zhou, K., & Wang, Z. 2023. Time parameter mapping and contour error precompensation for multiaxis input shaping. *IEEE Transaction on Industrial Informatics*. 19(3): 2640-51. DOI: 10.1109/TII.2022.3158960

[4] Ahumada, C. & Wheeler, P. 2021. Evaluation of input-shaping control robustness for the reduction of torsional vibrations. *IEEE Transactions on Industry Applications*. 57(5): 5028-38. DOI: 10.1109/TIA.2021.3087673

[5] Nguyen, M. N., Tran, D. T., & Ahn, K. K. 2018. Robust position and vibration control of an electrohydraulic series elastic manipulator against disturbance generated by a variable stiffness actuator. *Mechatronics*. 52: 22-35. DOI: 10.1016/j.mechatronics. 2018.04.004

[6] Ameura, H., Moal, P. L., Bourbona, G., Vuillemin, C., & Sworowski, M. 2022. Suppressing residual vibrations in comb-drive electrostatic actuators: a command shaping technique adapted to nomadic applications. *Sensors and Actuators A: Physical*. 334: 113366. DOI: https://doi.org/10.1016/j.sna.2022.113366

[7] Meng, L., Huang, Y., Wang, X., Li, F., & Li, H. 2020. Design and experimental validation of a robust input shaper for eliminating vibration in dielectric elastomer actuators under varying applied voltage. *Sensors and Actuators A: Physical*. 316: 112392. DOI: https://doi.org/10.1016/j.sna.2020.112392

[8] Smith, O. J. M. 1957. Posicast control of damped oscillatory systems. In *Proceedings of the IRE*. 1249-55. DOI: 10.1109/JRPROC.1957.278530

[9] Singer, N. C. & Seering, W. C. 1990. Preshaping command inputs to reduce system vibration. *Journal of Dynamic Systems, Measurement, and Control*. 112: 76-82. DOI: 10.1115/1.2894142

[10] Chatlatanagulchai, W., Damyot, S., & Intarawirat, P. 2017. Switching ZVDk input shaper for flexible closed-loop system with saturation. In *Proceedings of the American Control Conference*. 4492-7.

[11] Mohammed, A., Alghanim, K., & Andani, M. T. 2021. A robust input shaper for trajectory control of overhead cranes with non-zero initial states. *International Journal of Dynamics and Control*. 9(5): 230-9. DOI: https://doi.org/10.1007/s40435-020-00631-0

[12] Moonmanngmee, I., Juyploy, P., & Chatlatanagulchai, W. 2023. Input shaping for flexible systems with non-zero initial conditions. *Trends in Sciences*. 20(12). DOI: 10. 48048/ tis.2024.7193.

[13] Newman, D., Hong, S. W., & Vaughan, J. E. 2018. The design of input shapers which eliminate nonzero initial conditions. *Journal of Dynamic Systems, Measurement, and Control*. 140(10): 101005. DOI: https://doi.org/10.1115/1.4039668

[14] Wahrburg, A., Jurvanen, J., Niemelä, M., & Holmberg, M. 2022. Input shaping for non-zero initial conditions and arbitrary input signals with an application to overhead crane control. In *Proceedings of the IEEE 17th International Conference on Advanced Motion Control (AMC)*. 36-41. DOI: 10.1109/AMC51637.2022.9729261

[15] Thomsen, D. K., Søe-Knudsen, R., Brandt, D., Balling, O., & Zhang, X. 2019. Smooth online time-varying input shaping with fractional delay FIR filtering. *Control Engineering Practice*. 88(7): 21-37. DOI: 10.1016/j.conengprac. 2019.04.003

[16] Arabasi, S. & Masoud, Z. 2017. Simultaneous travel and hoist maneuver input shaping control using frequency modulation. *Shock and Vibration*. 2017(6): 5703820. DOI: https://doi.org/10.1155/2017/5703820

[17] Arabasi, S. & Masoud, Z. 2022. Frequency-modulation input-shaping strategy for double-pendulum overhead cranes undergoing simultaneous hoist and travel maneuvers. *IEEE Access*. 10(4): 44954-63. DOI: 10.1109/ACCESS.2022.3170099

[18] Chen, K. S., Yang, T. S., Ou, K. S., & Yin, J. F. 2009. Design of command shapers for residual vibration suppression in Duffing nonlinear systems. *Mechatronics*. 19(3): 184-198. DOI: 10.1016/j.mechatronics.2008. 08.005

[19] Chatlatanagulchai, W., Moonmanngmee, I., & Intarawirat, P. 2018. Input shaping for flexible system with nonlinear spring and damper. In *the ASME 2017 International Mechanical Engineering Congress and Exposition*.

[20] Tang W., Ma, R., Wang, W., & Gao, H. 2023. Optimization-based input-shaping swing control of overhead cranes. *Applied Sciences*. 13(17): 9637. DOI: 10.3390/app13179637

[21] Stein, A. & Singh, T. 2023. Minimum time control of a gantry crane system with rate constraints. *Mechanical Systems and Signal Processing*. 190(5): 110120. DOI: https://doi.org/10.1016/j.ymssp.2023.110120

[22] Nandi, S., & Singh, T. 2020. Joint chance constrained input shaping. *Journal of the Franklin Institute*. 357(9): 10027-53. DOI: 10.1016/j.jfranklin.2020.07.044

[23] Pilbauer, D., Michiels, W., & Vyhlídal, T. 2017. Distributed delay input shaper design by optimizing smooth kernel functions. *Journal of the Franklin Institute*. 354(9): 5463-85. DOI: 10.1016/j.jfranklin.2017.06.002

[24] Nithiuthai, S. & Chatlatanagulchai, W. 2019. Improved backstepping controller for rigid-flexible system using input shaping reference model matching and neural network. In *the 58th Annual Conference of the Society of Instrument and Control Engineers of Japan*. 1024-9. DOI: 10.23919/SICE.2019.8859811

[25] Chatlatanagulchai, W. 2017. Model reference input shaping using quantitative feedforward-feedback controller. *Engineering Journal*. 21(1): 207-20. DOI: 10.4186/ej.2017.21. 1.207.

[26] Yaovaja, K., Chatlatanagulchai, W., & Yaemprasuan, P. 2017. Anti-delay closed-loop input shaper to improve manual control of flexible system. In *Proceedings of the American Control Conference*. 4498 - 503. DOI: 10.23919/ACC.2017.7963648

[27] Ulriksen, M. D., Bernal, D., & Damkilde, L. 2018. Shaped input distributions for structural damage localization. *Mechanical Systems and Signal Processing*. 110(9): 499-508. DOI: 10.1016/j.ymssp.2018.03.039

[28] Park, J., & Schrader, C. B. Can an input shaper with two impulses suppress nonlinear residual vibrations? In *Proceedings of the American Control Conference*. 4492-7. DOI: 10.1109/ACC.2003.1244017

[29] Pelaez, G., Cararrini, N., & Garcia-Prada, J. C. 2007. Two-impulse sequence input shaper design for link mechanisms with nonlinearities. In *Proceedings of the American Control Conference*. 822-7. DOI: 10.1109/ACC.2007.4282326

[30] Masoud, Z. N. & Daqaq, M. F. 2006. A graphical approach to input-shaping control design for container cranes with hoist. *IEEE Transactions on Control Systems Technology*. 14(11): 1070-7. DOI: 10.1109/TCST. 2006.883194

[31] Masoud, Z. N. 2006. Oscillation Control of Quay-Side Container Cranes Using Cable-Length Manipulation. *Journal of Dynamic Systems, Measurement, and Control*. 129(7): 224-8. DOI: 10.1115/1.2432362

[32] Smith, J. Y., Kozak, K. C., & Singhose, W. E. 2002. Input shaping for a simple nonlinear system. In *Proceedings of the American Control Conference*. 821-826. DOI: 10.1109/ACC.2002.1024916

[33] Kozak. K. C. 2003. Robust command generation for nonlinear systems. *Ph.D. dissertation.* Department of Mechanical Engineering. Georgia Institute of Technology.

[34] Daqaq, M. F., Reddy, C. K., & Nayfeh, A. H. 2007. Input-shaping control of nonlinear MEMS. *Nonlinear Dynamics*. 54(3): 167-79. DOI: 10.1007/s11071-007-9246-x

[35] Chen, K. S., Yang, T. S., & Yin, J. F. 2006. Residual vibration suppression for duffing nonlinear systems with electromagnetical actuation using nonlinear command shaping techniques. *Journal of Vibration and Acoustics*. 128(12): 778-89. DOI: 10.1115/1.2203340